Available online at www.sciencedirect.com
SCIENCE DIRECT
Icarus 182 (2006) 513–526
ICARUS
www.elsevier.com/locate/icarus

Deep zonal winds can result from shallow driving in a giant-planet atmosphere

Adam P. Showman [a,*], Peter J. Gierasch [b], Yuan Lian [a]

[a] *Department of Planetary Sciences, Lunar and Planetary Laboratory, University of Arizona, Tucson, AZ 85721, USA*
[b] *Department of Astronomy, Cornell University, Ithaca, NY 14853, USA*

Received 7 July 2005; revised 10 December 2005

Available online 13 March 2006

Abstract

A simple model shows that acceleration of Jupiter and Saturn's multiple jets at altitudes confined near the top of the adiabatic region (e.g., at a few bars pressure) can produce jets that penetrate deeply into the molecular envelope. This result disproves the common assertion that jet acceleration near the outer margin can only produce zonal winds that are confined to these outer layers.

Keywords: Jupiter, atmosphere; Atmospheres, dynamics

1. Introduction

Two endpoint scenarios have been invoked for the vertical structure of Jupiter's ∼30 zonal jet streams. In the "shallow-structure" scenario, dubbed the "traditional view" by Ingersoll et al. (2004), the winds are confined to a thin region below the clouds. This scenario grew from analogy with the terrestrial ocean, which has weak currents near the bottom and strong currents near the top, and is broadly consistent with plausible constraints on subcloud temperatures (Ingersoll and Cuzzi, 1969). In the "deep-structure" scenario, the observed cloud-top winds are hypothesized to extend throughout the $\sim 10^4$ km-deep molecular envelope. This scenario evolved from the fact that Jupiter's interior is largely convective and hence thought to be adiabatic. On this basis, Busse (1976) suggested that the jets obey the Taylor–Proudman theorem throughout the interior, which implies that the jets would extend on cylinders parallel to the planetary rotation axis.

Two endpoint scenarios also exist for the mechanisms that drive the zonal jets (see Vasavada and Showman, 2005 for a detailed review). In the "shallow-forcing" scenario, the jets are pumped in the upper troposphere by turbulence injected at cloud level by moist convection, horizontal contrasts in solar heating (either equator-to-pole or band-to-band), or other cloud-layer processes (e.g., Barcilon and Gierasch, 1970; Gierasch et al., 1973; Gierasch, 1973, 1976; Williams, 1978, 1979, 2003; Ingersoll et al., 2000). In the "deep-forcing" scenario, convection cells that extend throughout the molecular hydrogen envelope (a depth of perhaps $\sim 10^4$ km) drive differential rotation in the interior that manifests as jets at the cloud level (e.g., Busse, 1976; Aurnou and Olson, 2001; Christensen, 2001, 2002).

Confusion exists in the literature over the relationship between these scenarios. Deep vs shallow *structure* models are rarely distinguished from the deep vs shallow *forcing* models, and numerous papers adopt the view that, if the jet acceleration occurs solely within the cloud layer (e.g., from solar energy or latent-heat release), then the resulting jets would remain confined within the cloud layer (e.g., Gierasch, 1976; Pollack et al., 1992; Atkinson et al., 1996, 1998; Seiff et al., 1997; Johnson, 2000; Young, 2003). Taken to an extreme, this view would imply that the wind profile could allow one to infer the forcing mechanism: shallow winds would imply shallow forcing while deep winds would imply deep (internal) forcing. Indeed, this assumption helped to motivate the Galileo probe Doppler wind experiment (Pollack et al., 1992), and the Probe's finding that the zonal winds extended to at least 22 bars, far below the depth

* Corresponding author. Fax: +1 (520) 621 4933.
E-mail address: showman@lpl.arizona.edu (A.P. Showman).

0019-1035/$ – see front matter
doi:10.1016/j.icarus.2006.01.019

of sunlight absorption, has been interpreted by many authors as implying a deep-convective origin for Jupiter's zonal winds (e.g., Atkinson et al., 1996; Seiff et al., 1997, 1998; Seiff, 2000; Folkner et al., 1997; Johnson, 2000). Young (2003) summarizes this view as follows:

> It is not impossible that [shallow] forcing could drive deeper winds from above. But if the winds are driven in the cloud layers, dynamical mechanisms must transport momentum from the upper levels downwards over at least 2–3 scale heights, and maybe many more scale heights depending on how deep the winds extend beyond 22 bars. No models have yet been constructed to identify dynamical modes that might accomplish such downward transport .... It seems more likely that the energy source for the winds comes principally from the interior heat flux, and that the cloud level winds are the upper extension of deeper convective wind fields, influenced by solar heating and perhaps latent heat release at cloud level.

From a dynamical point of view, the Taylor–Proudman theorem says nothing about *where* the winds are forced, and Atkinson et al. (1997) and Vasavada and Showman (2005) pointed out that deep winds obeying the Taylor–Proudman theorem could result from either deep or shallow forcing. If so, the existence of deep winds would not necessarily imply that the forcing is deep. However, this view is clearly not widespread, as the above literature survey demonstrates. Furthermore, the Taylor–Proudman theorem provides no insight into *how* a fluid would come to have deep winds from shallow forcing; it simply states that wind should not vary along the coordinate parallel to the rotation axis in a barotropic, geostrophically balanced fluid. Most importantly, the Taylor–Proudman theorem does not apply to statically stable fluids, which can support vertical shears of the zonal wind through thermal-wind balance (Holton, 2004, p. 70). The probable existence of static stability in Jupiter's cloud layer (Ingersoll et al., 2004) raises the question of whether deep winds can arise from shallow forcing in the presence of static stability.

The relative strength of shallow and deep forcing is unknown (Vasavada and Showman, 2005), but available constraints argue that they could be similar. Shallow and deep forcing are both ultimately driven by the same total heat flux of $\sim 10\ \mathrm{W\,m^{-2}}$. Heat-engine arguments suggest that the efficiency in converting this heat flux into kinetic energy in shallow circulations (e.g., thunderstorms or Hadley cells acting between 0.5–10 bars) may be similar, to within a factor of ~ 2, as the efficiency in converting the heat flux to kinetic energy in deep convection circulations. The implication is that the power per area generated by the two circulations may be comparable. This idea is supported by cloud-tracking observations of Beebe et al. (1980), Ingersoll et al. (1981), and Salyk et al. (2006), who suggest that shallow circulations are pumping eddy kinetic energy into the zonal jets at a rate $\sim 1\ \mathrm{W\,m^{-2}}$. The question is whether there is a *mechanism* by which this energy can drive deep jets.

Here, we present simple dynamical models demonstrating that deep zonal flow can indeed develop from momentum or thermal forcing that occurs only at the top of the troposphere (e.g., from latent-heat release or solar energy at pressures less than 10 bars). Section 2 investigates a neutrally stable (barotropic) model, and Sections 3 and 4 explore the influence of static stability in models with momentum and thermal forcing, respectively. The model dynamics are presented in the simplest possible form so the mechanisms that induce deep flow from shallow forcing can be identified. In reality, the forcing mechanisms may be deep, shallow, or both; any of these combinations may produce deep jets.

2. Jet spin-up and equilibration in a neutrally stable fluid: primitive-equation model

2.1. Model

We adopt the linearized primitive equations in pressure coordinates on an f-plane in Cartesian geometry. The zonal–momentum equation includes a Rayleigh-drag momentum forcing that relaxes the zonal winds to an assumed jet profile $u_F(y)$ over a timescale $\tau_F(p)$; this forcing provides a crude parameterization of the jet-pumping acceleration caused by cloud-layer processes such as moist convection (e.g., Ingersoll et al., 2000). Zonal symmetry is assumed; the dynamical variables are functions of northward distance y, pressure p, and time t. The geopotential and temperature are written $\Phi = \Phi_0 + \Phi'$ and $T = T_0 + T'$, respectively, where $\partial\Phi_0/\partial \ln p \equiv -RT_0$ is the hydrostatically balanced basic state (which depends on pressure only), R is the specific gas constant, and primed quantities are small perturbations from this basic state. We assume here that the domain lies within Jupiter's adiabatic interior and that no heating or cooling occurs, which implies that temperature remains constant on isobars and hence that $T' = 0$. No assumption is made about geostrophy. The equations can then be written

$$\frac{\partial u}{\partial t} = fv - \frac{u - u_F}{\tau_F(p)}, \tag{1}$$

$$\frac{\partial v}{\partial t} = -fu - \frac{\partial \Phi'}{\partial y}, \tag{2}$$

$$\frac{\partial \Phi'}{\partial \ln p} = -RT' = 0, \tag{3}$$

$$\frac{\partial v}{\partial y} + \frac{\partial \omega}{\partial p} = 0, \tag{4}$$

where u and v are zonal and meridional winds and $\omega \equiv \mathrm{d}p/\mathrm{d}t$ is vertical wind. A rigid boundary is adopted at the bottom, which leads to the boundary condition (e.g., Kalnay, 2003, p. 64)

$$\frac{\partial p_s}{\partial t} = -\int \frac{\partial v}{\partial y}\,\mathrm{d}p, \tag{5}$$

where p_s is the pressure at the bottom surface. At the crudest level, this boundary condition serves to bound the total fluid mass, which is crucial for obtaining deep jets from shallow forcing in finite time. The bottom boundary might represent an internal, statically stable layer or the base of the molecular region, where vertical fluid transport is inhibited.

To relate this basal pressure to the geopotential, note that the basal pressure-gradient acceleration $\rho_s^{-1}(\partial p_s/\partial y)_z$ can be expressed as $(\partial \Phi'/\partial y)_p$ (Holton, 2004, p. 58), where ρ_s is the basal density (constant for the weak, linear flows assumed here) and the subscripts z and p imply that the partial derivatives are taken at constant height and pressure, respectively. Equation (3) implies that Φ' is independent of pressure (and hence depends on y and t only), and Eq. (5) can then be converted to an equation for the time evolution of $\partial \Phi'/\partial y$.

To represent the pumping of alternating eastward and westward jets, we adopt a forcing speed that varies sinusoidally in latitude, $u_F = u_0 \cos ly$, where l is the latitudinal wavenumber of the jets that are being forced. The forcing timescale τ_F is taken as a constant, τ, at pressures less than $p_{\rm crit}$ and infinite at pressures exceeding $p_{\rm crit}$, which confines the jet pumping to pressures less than $p_{\rm crit}$ (i.e., the forcing equals zero in the deep layer). This assumption implies that if u and v do not initially depend on pressure (e.g., if they are zero), then they remain piecewise constant with pressure (around $p_{\rm crit}$) for all time. Equations (1), (2), and (5) then admit solutions $u = U(p,t)\cos ly$, $v = V(p,t)\cos ly$, and $\Phi' = \phi(t)\sin ly$, where

$$U(p,t) = \begin{cases} u_{\rm top}(t), & p \leqslant p_{\rm crit}, \\ u_{\rm bot}(t), & p > p_{\rm crit}, \end{cases}$$

$$V(p,t) = \begin{cases} v_{\rm top}(t), & p \leqslant p_{\rm crit}, \\ v_{\rm bot}(t), & p > p_{\rm crit}. \end{cases}$$

Equations (1), (2), and (5) then collapse to a set of five coupled ordinary-differential equations for the winds and geopotential

$$\frac{{\rm d}u_{\rm top}}{{\rm d}t} = f v_{\rm top} - \frac{u_{\rm top} - u_0}{\tau}, \tag{6}$$

$$\frac{{\rm d}v_{\rm top}}{{\rm d}t} = -f u_{\rm top} - l\phi, \tag{7}$$

$$\frac{{\rm d}\phi}{{\rm d}t} = \frac{l}{\rho_s}(v_{\rm top}\Delta p_{\rm top} + v_{\rm bot}\Delta p_{\rm bot}), \tag{8}$$

$$\frac{{\rm d}u_{\rm bot}}{{\rm d}t} = f v_{\rm bot}, \tag{9}$$

$$\frac{{\rm d}v_{\rm bot}}{{\rm d}t} = -f u_{\rm bot} - l\phi. \tag{10}$$

Here, $\Delta p_{\rm top} = p_{\rm crit}$ and $\Delta p_{\rm bot} = p_s - p_{\rm crit}$ are the pressure ranges corresponding to the two layers. Equations (6)–(10) are solved numerically using a fourth-order Runge–Kutte scheme.

2.2. Results

The numerical solutions show that, because of the upper-level forcing, the zonal wind accelerates in both the upper and lower layers, leading to a barotropic structure with zonal winds that extend far below the forcing region. Fig. 1 illustrates this process for a case with zero initial geopotential perturbation and winds, a forcing speed of $u_0 = 30\ {\rm m\,s^{-1}}$, and a forcing timescale of $\tau = 10^7$ s. This timescale is motivated by Voyager and Cassini observations, which suggest that eddies drive the jets at cloud level with a characteristic pumping time of 10^7 s (Beebe et al., 1980; Ingersoll et al., 1981; Salyk et al., 2006). In this example, the domain extends to 100 bars, but the forcing is confined to pressures less than 1 bar. Once the forcing begins, the upper and lower-level winds accelerate in tandem (Figs. 1a and 1b), and the difference between them never exceeds $\sim 0.02\ {\rm m\,s^{-1}}$. The zonal winds converge toward a steady state value of u_0 with a characteristic timescale of 10^9 s (30 years), which is 10^2 times greater than the forcing timescale τ. The meridional velocities quickly reach $\sim 0.02\ {\rm m\,s^{-1}}$ in the upper layer (Fig. 1c), but they are only $\sim 0.0002\ {\rm m\,s^{-1}}$ in the lower layer, and they gradually decline toward zero in both layers as the steady state develops. The perturbation geopotential gradually increases, maintaining approximate geostrophic balance with the zonal winds, and converges toward a steady state with a ~30-year timescale. Identical cases initialized with different initial conditions converge to the same

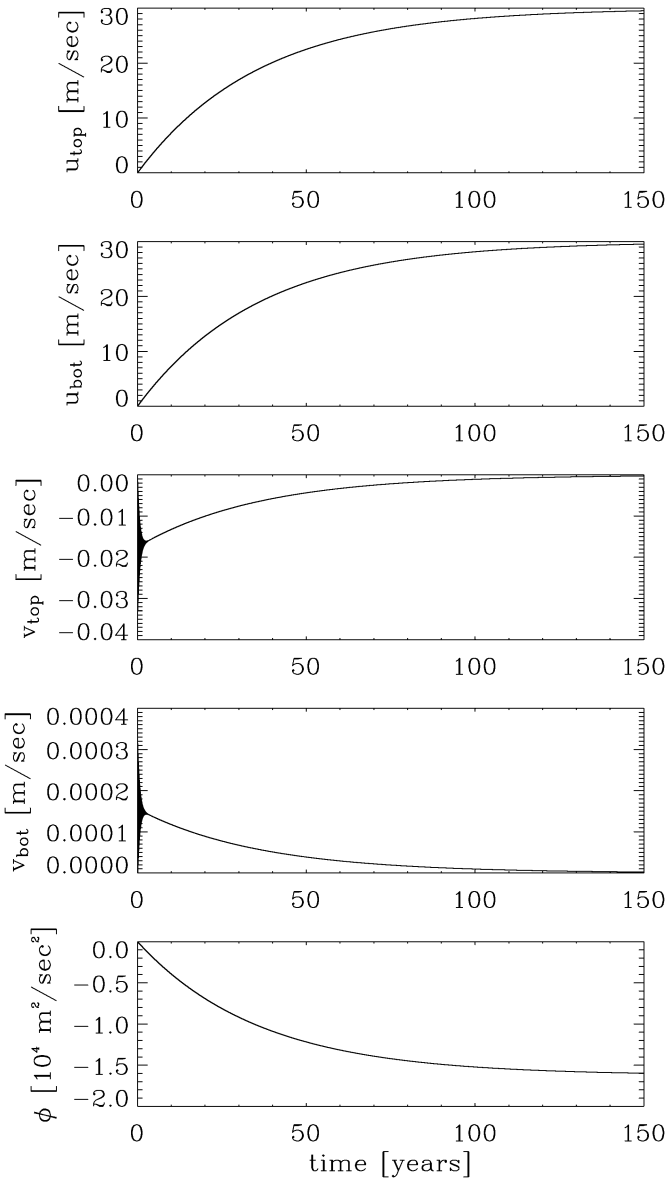

Fig. 1. Winds and geopotential for a neutrally stable model with $\tau = 10^7$ s, $p_{\rm crit} = 1$ bar, and a domain extending to 100 bars. $\rho_{\rm bot} = 4.64\ {\rm kg\,m^{-3}}$, $f = 1.7 \times 10^{-4}\ {\rm s^{-1}}$, $l = 3.14 \times 10^{-7}\ {\rm m^{-1}}$ (corresponding to a jet width of 10^4 km). Shallow jet forcing drives deep, barotropic zonal jets.

steady state over similar timescales, indicating the insensitivity of the final state—including the fast deep winds—to initial condition. Furthermore, when the domain bottom is increased to 10^3 or 10^4 bars, the fluid converges to the same barotropic steady state, but the e-folding time to reach this steady state increases to 10^{10} and 10^{11} s (300 and 3000 years), respectively.

The nonzero meridional wind illustrated in Fig. 1 implies that an overturning circulation develops in the latitude-height plane. The vertical wind associated with this circulation can be obtained by integrating Eq. (4) from the bottom boundary condition $\omega_{\rm bot} = \partial p_s/\partial t$. This leads to the expressions

$$\omega(y,p,t) = \begin{cases} \omega_{\rm bot} - l\sin ly\big[\Delta p_{\rm bot} v_{\rm bot} \\ \quad + (p_{\rm crit} - p)v_{\rm top}\big], & p \leqslant p_{\rm crit}, \\ \omega_{\rm bot} - l\sin ly(p_s - p)v_{\rm bot}, & p > p_{\rm crit}, \end{cases} \tag{11}$$

where $\omega_{\rm bot} = \rho_{\rm bot}\sin ly\,\partial\phi/\partial t$. A streamfunction ψ for this circulation can be defined by the expressions $v = -\partial\psi/\partial p$ and $\omega = \partial\psi/\partial y$, which yields

$$\psi = \begin{cases} \cos ly\big[\Delta p_{\rm bot} v_{\rm bot} + (p_{\rm crit} - p)v_{\rm top} \\ \quad - (\rho_{\rm bot}/l)\partial\phi/\partial t\big], & p \leqslant p_{\rm crit}, \\ \cos ly\big[(p_s - p)v_{\rm bot} - (\rho_{\rm bot}/l)\partial\phi/\partial t\big], & p > p_{\rm crit}. \end{cases} \tag{12}$$

Fig. 2 illustrates this meridional circulation with contours (showing streamfunction) and arrows (showing v, ω velocity). At pressures less than 1 bar, the overturning is southward at eastward jets and northward at westward jets; the directions are reversed at pressures exceeding 1 bar. Ascent and descent occur at the north and south edges, respectively, of eastward jets. The zonal winds (greyscale) develop an alternating pattern of east–west jets that extend barotropically to the base of the fluid.

The spinup of the deep jets, despite the lack of deep forcing, results from the development of the meridional overturning circulation shown in Fig. 2. When the jet pumping begins at $p < p_{\rm crit}$, an upper-level zonal wind develops, and the Coriolis force on the growing zonal wind induces a meridional flow at the level of the forcing. In the northern hemisphere, this flow is southward at eastward jets and northward at westward jets, which causes upper-level convergence at the southern edge of eastward jets (northern edge of westward jets). This upper-level convergence increases the fluid mass per area in these regions, which, through hydrostatic equilibrium, causes pressure to increase on constant-height surfaces *throughout the depth of the fluid*. Similarly, upper-level divergence occurs at the northern edges of eastward jets (southern edges of westward jets), which causes pressure to decrease on constant-height surfaces throughout the fluid depth. The upper-level meridional flow thereby induces barotropic pressure gradients, and these in turn drive a lower-layer meridional flow that is opposite in sign to the upper-layer flow (in the lower layers, fluid moves from pressure highs to lows, which in the northern hemisphere implies northward flow underneath the eastward jets and southward flow underneath westward jets). Coriolis accelerations on this lower-layer meridional flow then induce a lower-layer zonal flow with the same sign as the upper-layer zonal flow. A barotropic zonal flow therefore develops despite the fact that the jet pumping in Fig. 2 occurs only in the top 1% of the fluid mass.

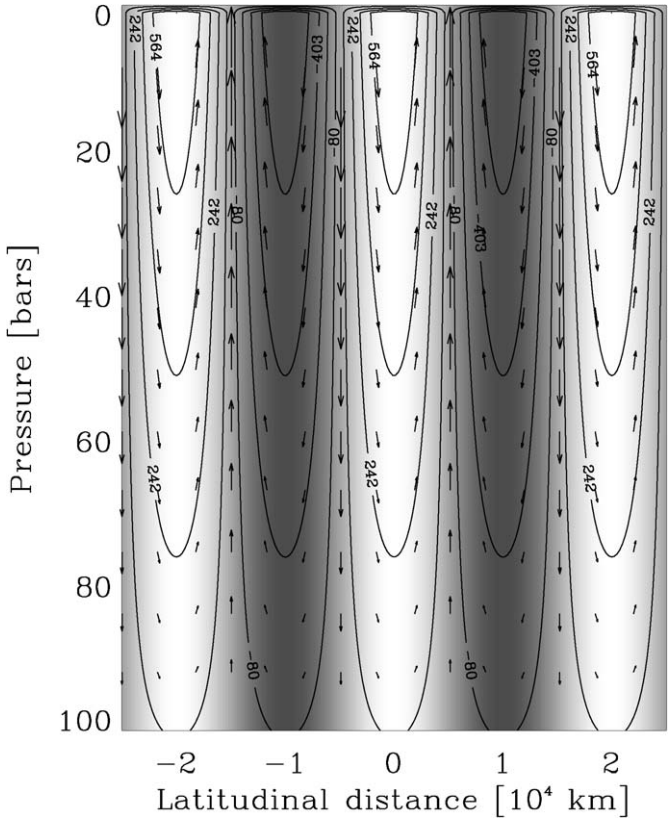

Fig. 2. Snapshot of the flow from the simulation in Fig. 1 at 30 years. Greyscale depicts zonal wind, which ranges from 17 m s^{-1} (eastward) in white to −17 m s^{-1} (westward) in black. Contours show streamfunction of the meridional circulation. The overturning speed is inversely proportional to spacing between contours, which is large at pressures less than 1 bar and small at pressures exceeding 1 bar. Arrows show the (v,ω) velocity of the meridional circulation at $p > 1$ bar. At $p < 1$ bar, the meridional circulation flows the other way and is approximately 100 times stronger than in the deeper layer.

In Fig. 2, the deep-layer meridional velocities reach $\sim 10^{-4}$–10^{-5} m s^{-1}, which is smaller than probable convective velocities in Jupiter's interior of ~ 0.1 m s^{-1}. One could wonder whether this mismatch in velocities would prevent a coherent meridional circulation from forming in the deep layer. We argue that the answer is no. In atmospheres, the instantaneous meridional velocities generally exceed the time-averaged ones, but this does not imply that the time-mean flow, while weak, is disrupted or lost. If the upper-layer flow causes a net, time-averaged horizontal divergence in the upper layer, then mass continuity demands that this *must* be balanced by a net, time-averaged horizontal convergence in the lower layer—even if this convergence is weak compared to instantaneous motions.

The structure of Eqs. (6)–(10) and the behavior shown in Fig. 1 suggest the possibility of an analytic solution. Adopting solutions in $(u_{\rm top} - u_0)$, $v_{\rm top}$, $(u_{\rm bot} - u_0)$, $v_{\rm bot}$, and $(\phi - fu_0/l)$ proportional to $e^{i(\sigma_r + i\sigma_i)t}$ leads to two coupled fifth-order polynomial equations for the real and imaginary frequencies σ_r and σ_i (corresponding to oscillations and exponential growth/decay of the solutions, respectively). These equations do not have general analytical solutions; however, in the limit where $\sigma_i \ll \tau^{-1} \ll f$, $\Delta p_{\rm bot}/\Delta p_{\rm top} \to \infty$, and $\sigma_r = 0$, the solution corresponds to exponential decay toward the barotropic steady state

with a timescale

$$\sigma_i^{-1} = \frac{\tau \Delta p_{\rm bot}}{\Delta p_{\rm top}}. \tag{13}$$

This behavior confirms our numerical simulations and implies that the e-folding time to spin up the entire fluid into the barotropic final state is simply τ times the ratio of the total fluid mass to the fluid mass experiencing direct forcing. The other modes do not generally have analytic solutions; several of them correspond to ageostrophic standing waves. (In Fig. 1, such a mode in v becomes excited, and then damps out, during the first ∼3 years.)

3. Stably stratified model with momentum forcing

Evidence suggests that static stability exists within the cloud layer near ∼1 bar. Analysis of Galileo probe measurements give subadiabatic gradients of ∼1–2 K per scale height between 1 and 20 bars (Magalhães et al., 2002). Studies of mesoscale waves on Jupiter suggest that a layer near or just below the visible clouds has a Richardson number on the order of unity, implying stable stratification (Flasar and Gierasch, 1986; Bosak and Ingersoll, 2002). Studies of equatorial plumes, hot spots, and the expanding ring observed after the Comet Shoemaker–Levy 9 impact all implicate waves that require static stability to propagate (Allison, 1990; Ingersoll and Kanamori, 1995; Ortiz et al., 1998; Showman and Dowling, 2000; Friedson, 2005). Such static stability could arise directly from latent heating associated with the condensation of water from ∼1–10 bars (Achterberg and Ingersoll, 1989; Nakajima et al., 2000) or by the action of sloping convection (e.g., baroclinic or inertial instabilities) in the presence of lateral temperature contrasts between belts and zones. Several studies suggest a complex vertical structure with a nearly neutral layer in the upper troposphere (∼0.5–2 bars) underlain by a stable layer somewhere between ∼2 and 20 bars (e.g., Allison, 1990, 2000; Allison and Atkinson, 2001; Achterberg and Ingersoll, 1989; Ingersoll and Kanamori, 1995). In contrast, the deep interior loses heat primarily by convection and therefore has nearly zero static stability. Nevertheless, the internal convection dynamics or compositional effects might produce a small but positive stratification even in deep regions (e.g., Turner, 1979, pp. 221–222).

It is therefore of interest to ask how a positive stratification affects the downward penetration of jets forced near the top of the system. This question can be addressed with a modification of the model described in Section 2. As previously, a basic state temperature profile $T_0(p)$ is assumed, but it is now stratified. We express the stratification in terms of the Brunt frequency N, given by

$$N^2 = \frac{g}{H}\left(\frac{R}{c_p} - \frac{p}{T_0}\frac{{\rm d}T_0}{{\rm d}p}\right), \tag{14}$$

where $H = RT_0/g$. The modified governing equations are

$$\frac{\partial u}{\partial t} - fv = \frac{u_F - u}{\tau_F}, \tag{15}$$

$$fp\frac{\partial u}{\partial p} = R\frac{\partial T'}{\partial y}, \tag{16}$$

$$\frac{\partial v}{\partial y} + \frac{\partial \omega}{\partial p} = 0, \tag{17}$$

$$\frac{\partial T'}{\partial t} - \frac{N^2H^2}{Rp}\omega = \frac{T'_E - T'}{\tau_R}. \tag{18}$$

This is the same set of balances frequently used to study the zonal mean structure of the terrestrial middle atmosphere (Holton, 2004, chap. 12). The neglect of advection in the momentum equations is valid because the advection terms are order Ro smaller than the pressure-gradient and Coriolis terms, where $Ro \sim 0.05$ is the Rossby number (i.e., the balance is geostrophic). In the thermodynamic-energy equation (18), we neglected horizontal temperature advection but included vertical advection of the background stratification (right term on the left side). This assumption is approximately valid as long as the actual temperature perturbations T' are small compared to the temperature deviations (relative to a dry adiabat) associated with the background stratification. This condition is satisfied to a factor of ∼2–3 for most of the parameter ranges we consider.

We set T'_E to zero so that radiation forces the fluid toward the basic-state temperature T_0, which depends on pressure but not latitude. The jet forcing u_F will be nonzero only within a top layer, as previously. We have assumed geostrophic balance in the meridional direction. The transients that develop if this assumption is not made have already been discussed and it is simplest to assume balance while investigating stratification effects. The radiative (τ_R) and frictional drag (τ_F) adjustment time scales are parameters that can be functions of pressure. We retain the time derivatives $\partial u/\partial t$ and $\partial T'/\partial t$ so that the time scale for adjustment to equilibrium can be investigated.

Equations (15)–(18) form a complete set for the four unknowns T', u, v and ω. Boundary conditions are that $\omega = 0$ at the top and bottom pressure surfaces. We will use the system two ways. First, we wish to investigate the steady-state equilibrium for forced solutions, for which u_F is nonzero within a layer near the top of the system. Secondly, we want to investigate the time scale for decay of free solutions, and therefore the time scale for establishment of an equilibrium after u_F has been imposed or altered. Since all coefficients are constant in time, we expect decay of free solutions to take the form $\exp(-\gamma_n t)$, where the subscript n indicates that there may be a spectrum of decay-rate eigenvalues associated with different spatial modes. This turns out to be the case. To simplify manipulations while reducing (15)–(18) to one equation, it is useful to exploit this simple time dependence by writing

$$D_F = \frac{\partial}{\partial t} + \frac{1}{\tau_F} = \gamma + \frac{1}{\tau_F} \quad \text{and} \quad D_R = \frac{\partial}{\partial t} + \frac{1}{\tau_R} = \gamma + \frac{1}{\tau_R}. \tag{19}$$

Then combining (15)–(18) gives a single equation for the meridional streamfunction

$$\frac{N^2H^2}{f^2}\frac{\partial^2\psi}{\partial y^2} + p^2 D_R \frac{\partial}{\partial p}\left(\frac{1}{D_F}\frac{\partial \psi}{\partial p}\right) = \frac{p^2}{gf} D_R \frac{\partial}{\partial p}\left(\frac{u_F}{\tau_F D_F}\right). \tag{20}$$

As Holton (2004) discusses, the elliptic operator on the left-hand side produces a ratio between horizontal and vertical length scales, with greater vertical penetration when the parameter N^2H^2/f^2 is smaller. For a qualitative investigation of this behavior in the Jupiter regime we adopt a simple case with τ_F, τ_R, and N^2H^2 piecewise constant in two layers. If the latitudinal dependence of u_F is assumed proportional to $\cos ly$, as in Section 2, Eq. (20) then separates and leads to an ordinary differential equation for the pressure dependence. Then if u_F is also assumed piecewise constant in two layers (specifically, zero in the deep layer), the right-hand side of Eq. (20) becomes a delta function located at the interface pressure. The solutions to the homogeneous equations within each layer are simple powers of pressure. Coefficients are determined from interface and boundary conditions.

By setting $\partial/\partial t = \gamma = 0$ we can investigate the steady equilibrium solutions to Eq. (20). The appropriate Brunt frequency is of course unknown and we experiment with a range of values. To explore the dependence of zonal-wind penetration depth on stratification, we examined two series of solutions: one where N is held constant with depth throughout the fluid and another where N is large in the upper (forced) layer and small in the lower (unforced) layer. In all cases, we adopt numbers crudely representative of Jupiter: $f = 1.8 \times 10^{-4}$ s^{-1} (30° latitude) and $l = 5 \times 10^{-7}$ m^{-1}, corresponding to a latitudinal wavelength of about 12,600 km. We take $u_F = 100$ m s^{-1} in the top layer and zero at depth. In Section 2 only the mass in each layer was important, and for simplicity the pressure at the top was taken to be zero. Here we wish to avoid a singularity at $p = 0$, and we adopt a top layer extending from 1 to 5 bars and a deep layer from 5 bars to 1000 bars.

Fig. 3 displays vertical structure results when N is held constant with depth at 2×10^{-3}, 2×10^{-4}, 2×10^{-5}, and 2×10^{-6} s^{-1} in the top through bottom rows, respectively. These cases adopt $H = 100$ km and use frictional time constants of 1 and 100 years in the top and bottom layers and radiative time constants of 100 and 10^4 years in the top and bottom layers. As the stratification becomes smaller, the meridional streamfunction, the zonal wind and the temperature perturbation all penetrate more deeply. The amplitude of the temperature perturbation decreases as N decreases. Consistent with the thermal wind equation, the vertical shear decreases and the zonal flow becomes deeper. In the bottom row of panels, for which the stratification is smallest, the wind is almost uniform in height. Its value, about 28.7 m s^{-1}, is consistent with the pressure-weighted frictional damping rate for the combined two-layer system. An otherwise similar case but with no frictional damping in the bottom layer (not shown) reaches equilibrium with $u = 100$ m s^{-1}, and is analogous to the equilibrium solutions of the barotropic model in Section 2.

Fig. 4 displays the behavior when the stratification is held at a large value in the top layer and a smaller value in the bottom layer. This set addresses the outer planet situation somewhat more realistically, since observations suggest that tropospheric levels on Jupiter, even as deep as the one bar level or more, are stably stratified, whereas the deep interior is probably closer to neutral. Several authors have suggested that the stability increases with depth in the upper troposphere before decreasing again in the convective interior, and this could conceivably be modeled with a structure containing three or more layers. However, our basic goal here is simply to determine the effect of upper-tropospheric static stability on a more neutrally stratified interior, and a two-layer model suffices for this purpose (the stability in the upper layer then represents a vertical average over any small-scale structure that exists). Because the deep-interior properties are poorly known, we vary the deep layer stratification in this series of experiments.

Parameters are chosen to crudely represent Jupiter. In the upper layer (one to five bars), $N = 2 \times 10^{-3}$ s^{-1} for all cases (as might be expected from latent-heat release associated with condensation of a solar abundance of water). In the deeper layer (5–1000 bars), $N = 10^{-3}$ s^{-1} in the top row of panels (Fig. 4), and is reduced successively by a factor of 10 in the second, third, and fourth (bottom) rows. The smallest stratification corresponds to fractional-temperature deviations from an adiabat of only $\sim 10^{-6}$ over vertical distances of 10^4 km. This is comparable to the expected deviation from an adiabat caused by convection in Jupiter's interior. Scale heights of 25 and 100 km are used in the top and bottom layers. Frictional and radiative time constants are 1 and 10 years in the top layer and 100 and 1000 years in the bottom. The results show that the deep region becomes increasingly barotropic (with decreasing vertical shear) as the deep stratification is reduced. The top layer remains baroclinic, in contrast to the results in Fig. 3, where the entire system becomes barotropic in the limit of small stratification.

Fig. 5 illustrates the complete flow geometry for the case of Fig. 4, second row (which has $N = 10^{-4}$ s^{-1} at depth). Fig. 5 is similar to Fig. 2 but it is important to point out that in Fig. 5, with frictional and radiative damping, the meridional circulation represents a steady flow in equilibrium with the forcing u_F. The frictionless deep flow model illustrated in Fig. 2 has a similar meridional flow structure, but it only persists while the deep flow is accelerating. In Fig. 5, the zonal winds decrease by a factor of two from 1 to $\sim$12 bars, but a substantial barotropic zonal wind extends from 12 bars to the model bottom at 1000 bars despite the confinement of jet forcing to pressures less than 5 bars.

In the models discussed here, as with those from Section 2, Coriolis accelerations on the upper-layer forcing induce a meridional circulation that penetrates below the forcing region. Because of the static stability in the case here, however, the ascent and descent associated with the overturning push the temperature away from the basic state. (Advection of high-entropy air from above makes descending regions hot; advection of lower-entropy air from below makes ascending regions cold.) Because ascent and descent occur on the poleward and equatorward sides of eastward jets, respectively (equatorward and poleward sides of westward jets, respectively), these are exactly the temperature gradients needed to allow the upper-level zonal wind to decay with depth according to the thermal-wind equation. The *rate* of decay of the winds with depth (i.e., vertical gradient of zonal wind), however, depends on the magnitude of temperature perturbations (deeper jet penetration occurs for smaller temperature perturbations). Large stability allows for-

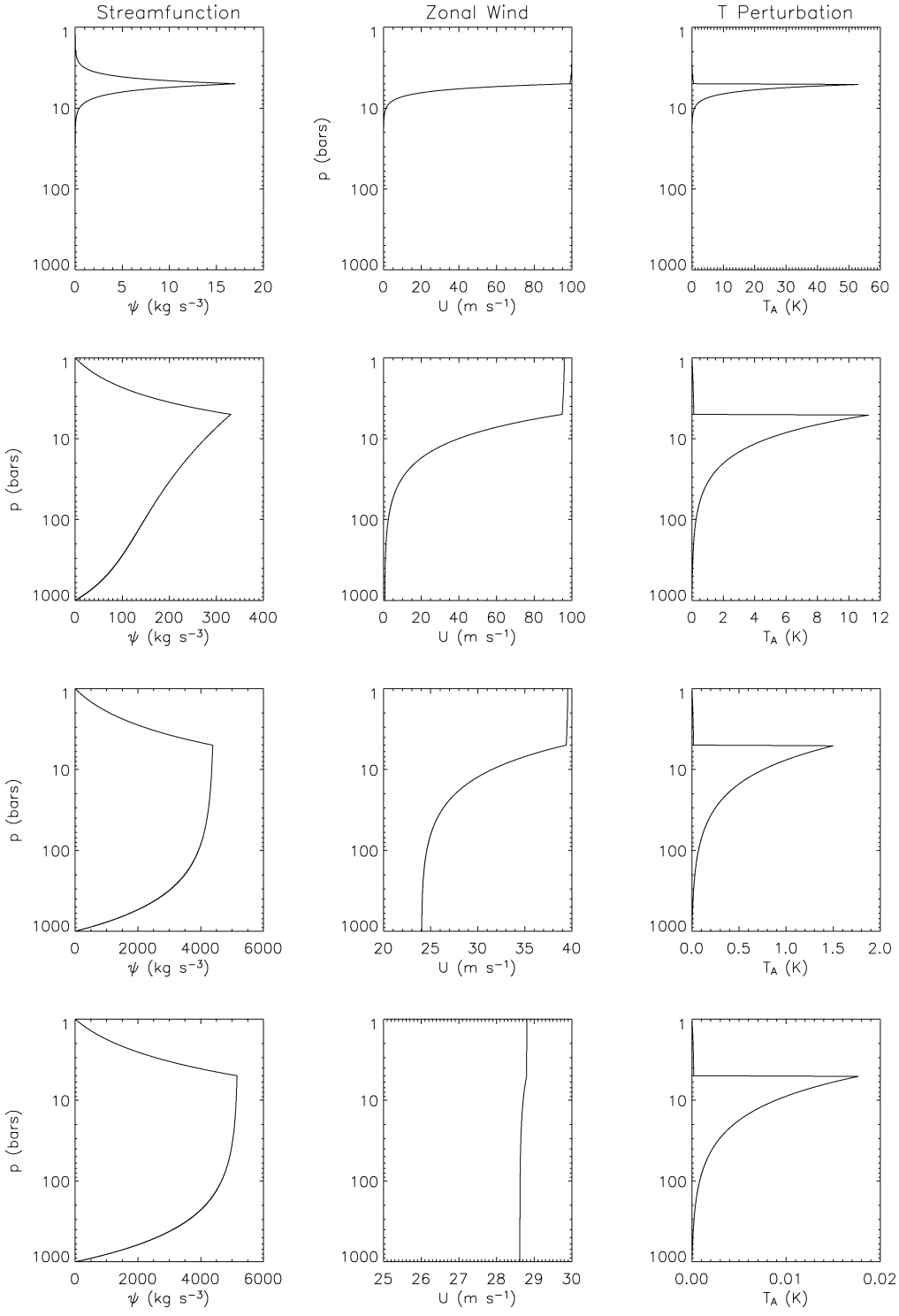

Fig. 3. Effect of static stability in a model with momentum forcing. Each of the four rows shows the results of a model. In each model the Brunt frequency is constant with height, given by $N = 2 \times 10^{-3}$, 2×10^{-4}, 2×10^{-5}, and 2×10^{-6} s^{-1} in first (top), second, third, and fourth (bottom) rows, respectively. From left to right, the panels show the pressure dependence of the streamfunction, zonal wind, and temperature perturbation. Note that the full two-dimensional streamfunction, zonal wind, and temperature perturbation (which are functions of latitude and pressure) are obtained by multiplying the curves shown by a sine or cosine in latitude (see text). Similar comments apply to Figs. 4 and 7.

mation of large temperature perturbations from ∼5–100 bars (top two rows of Figs. 3, 4), so the wind decays rapidly with depth in the deep layer. In contrast, small stability strongly limits the magnitude of temperature perturbations that can result from vertical advection, even when the overturning is vigorous (bottom two rows of Figs. 3 and 4); therefore, zonal winds in the deep layer, if any, decay only weakly with depth. Small stability also promotes the existence of deep zonal winds by allowing stronger meridional overturning (notice how the streamfunction values in Figs. 3 and 4 increase as stability is decreased).

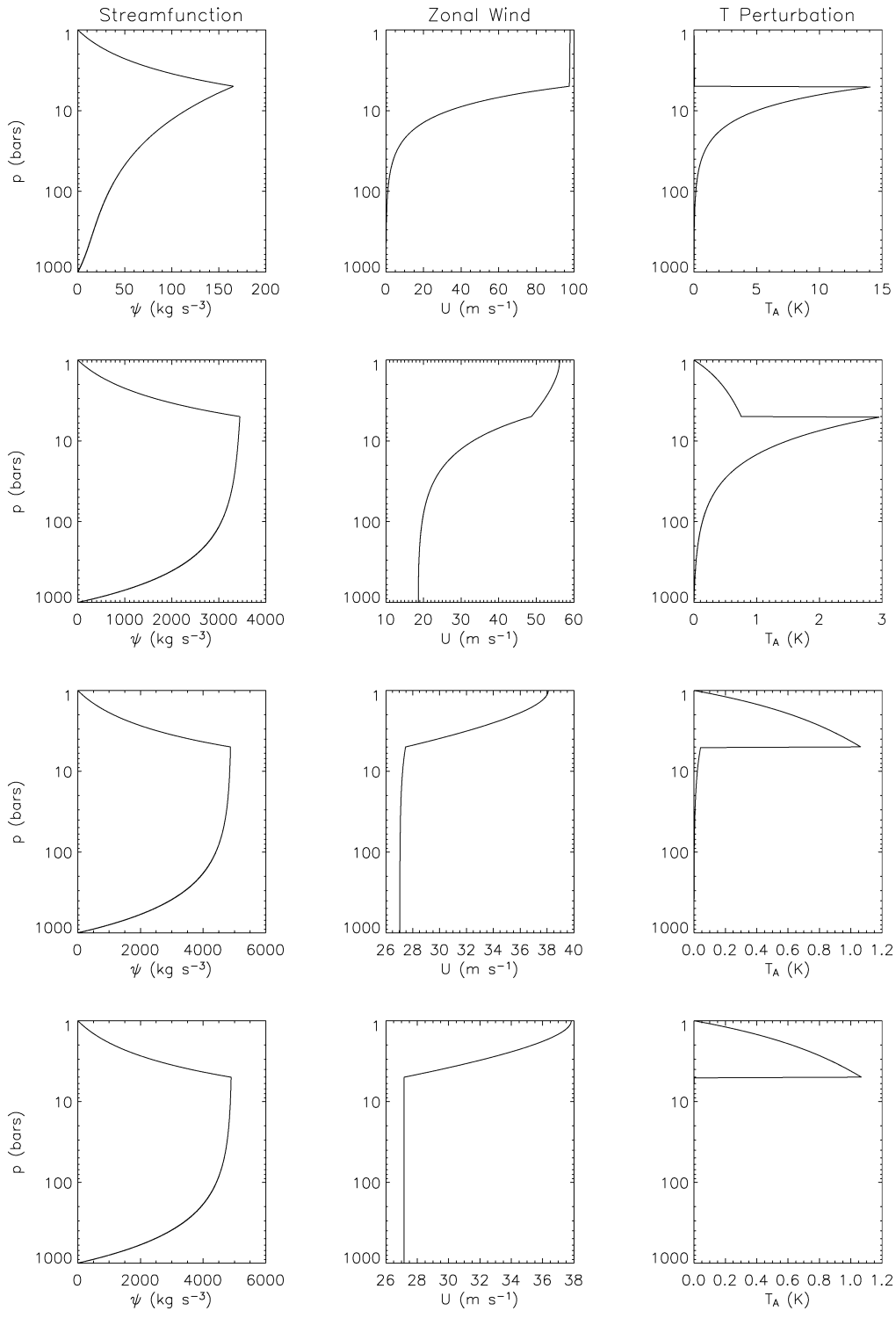

Fig. 4. Effect of static stability in a two-layer model with momentum forcing. As in Fig. 3, each row shows the results of an experiment. The Brunt frequency in the top layer is held at $N = 2 \times 10^{-3}$ s^{-1} in all cases shown. In the deep layer it is $N = 10^{-3}$, $N = 10^{-4}$, $N = 10^{-5}$, and $N = 10^{-6}$ s^{-1} from the top to bottom rows of the figure. Shown from left to right are the streamfunction, zonal wind, and temperature perturbation. Even in the presence of a statically stable upper layer, shallow momentum forcing can drive deep jets as long as the deep-layer static stability is small.

Stronger meridional overturning leads to stronger Coriolis accelerations in the deep fluid, which in turn leads to greater pumping of deep jets. Thus, when the deep stability is small, two distinct factors promote the formation of a nonzero deep wind: the small temperature perturbations require small vertical shear of the deep-zonal wind (i.e., the deep zonal wind is nearly constant), and the faster meridional overturning allows more vigorous Coriolis acceleration of the deep-zonal wind (implying that the near-constant zonal wind that develops is nonzero).

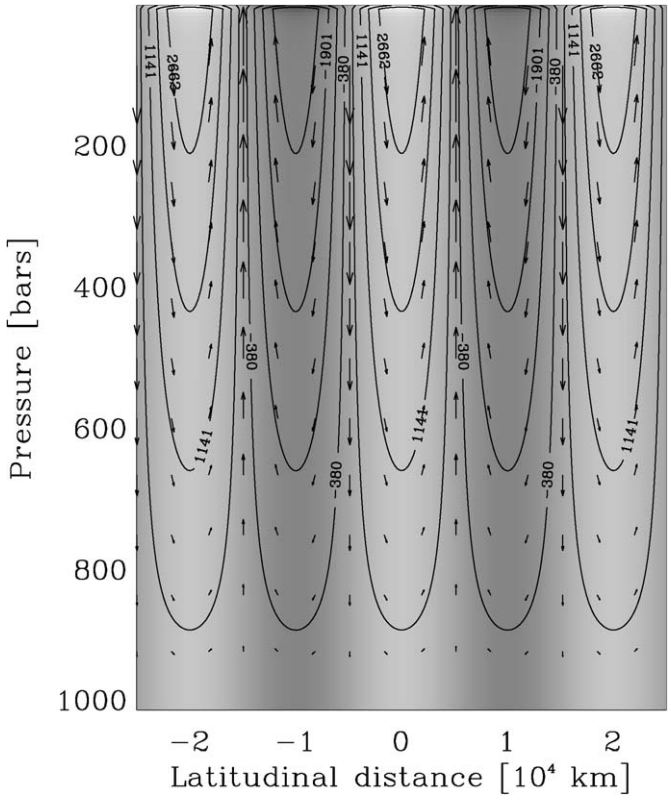

Fig. 5. Flow geometry for the case of Fig. 4, second row of panels. Labeling is the same as in Fig. 2. Notice the deep penetration of the meridional overturning cells and zonal winds even though the forcing region (from 1–5 bars) is statically stable.

In summary, the basic requirement for deeply penetrating zonal winds is simply that the meridional circulation (caused by the upper-layer forcing) penetrate deeply into the interior. One of our most interesting results is that such deep penetration occurs even in the presence of strong static stability in the upper *forced* layer, as long as the deeper *unforced* layer has small static stability. This is precisely the expected stability structure for Jupiter, which implies that deep winds on Jupiter could result from forcing associated with latent-heat release (e.g., Ingersoll et al., 2000) or sunlight (e.g., Williams, 2002, 2003) near the top of the system.

In our model, the steady-state jet strengths in the deep layer depend on the ratio of the frictional time constants in the bottom and top layers, $\tau_F^{\rm bot}/\tau_F^{\rm top}$. Because the bottom layer contains much more mass than the top layer, the top-layer meridional wind speeds exceed those in the bottom layer by a factor $\Delta p_{\rm bot}/\Delta p_{\rm top} \gg 1$. As a result, the east–west Coriolis accelerations (which provide the jet acceleration in the bottom layer) are much weaker in the bottom layer than in the top layer. When $\tau_F^{\rm bot} \gg \tau_F^{\rm top}$, this presents no problem, because the weak jet acceleration in the bottom layer is only weakly resisted by friction, allowing fast jets to develop in the bottom layer. If $\tau_F^{\rm bot} \sim \tau_F^{\rm top}$, however, then the weak jet acceleration in the bottom layer is resisted by strong frictional damping, leading to equilibrated deep-layer winds that are much smaller than u_F.

Available constraints, however, argue that $\tau_F^{\rm bot}/\tau_F^{\rm top} \gg 1$, which suggests that fast deep jets can indeed result from shallow forcing. Cloud-tracking observations suggest that eddies tilt into the jet shear at the ∼1-bar level, accelerating the jets with a characteristic timescale of ∼1 year at the cloud layer (Beebe et al., 1980; Ingersoll et al., 1981; Salyk et al., 2006). This motivates our choice of $\tau_F^{\rm top} \sim 1$ year in Figs. 3 and 4. No observational constraints exist on friction timescales in the deep atmosphere, but mixing-length theory can provide a crude estimate. In rotationally dominated flows, convective velocities tend to scale as $w \sim [\alpha g F/(\rho c_p \Omega)]^{1/2}$, where α, g, F, ρ, c_p, and Ω are thermal expansivity, gravity, heat flux, density, specific heat, and planetary rotation rate (e.g., Fernando et al., 1991). Using jovian parameter values at 100 bars implies $w \sim 0.1\ {\rm m\,s^{-1}}$. If the sole effect of these convective motions on the zonal jets is to induce diffusive damping, then mixing-length theory (e.g., Cox and Giuli, 1968) yields an eddy viscosity $\nu \sim wH$, where H is the local scale height. The time for friction to decelerate the jets is then L^2/ν, which is $\sim 10^2$–10^3 years for a jet width $L \sim 10^4$ km and $w \sim 0.1\ {\rm m\,s^{-1}}$. This estimate motivates our choice of $\tau_F^{\rm bot} = 100$–1000 years in Figs. 3, 4, 5, and 7. Mixing-length theory probably provides only a lower limit on the friction time constant, however. For example, the latitudinal potential-vorticity gradients associated with jets discourages latitudinal mixing (Bartello and Holloway, 1991), which would lead to smaller eddy viscosities than suggested here. More importantly, turbulence may not act in a diffusive manner; for example, turbulence can transport momentum *into* jets rather than away from them, which can be represented as a *negative* eddy viscosity. This tendency competes with any tendency for turbulence to damp the jets, and depending on the relative roles of up-gradient and down-gradient momentum transfer, the net frictional timescale could potentially exceed those suggested by mixing-length theory by orders of magnitude.

Interestingly, as $\tau_F^{\rm bot} \to \infty$, the steady-state solution is $v = \omega = T' = 0$ and $u = u_F$ throughout. In this case, the lack of deep-layer friction prevents a steady-state meridional circulation in the deep layer, and continuity then prevents a meridional circulation in the top layer too. (One could wonder whether, in this case, meridional circulations could still occur within the top layer but not the bottom layer. The answer is no: in this model, the return branch of the meridional flow, if any, *must* occur in the bottom layer. In other words, the sign reversal in the profile of v versus pressure occurs at the interface between the layers, which can be seen from the fact that the sign reversal in the slope of the streamfunction in Figs. 3 and 4 occurs at the interface pressure. Therefore, a suppression of the deep-layer meridional circulation implies a suppression of the top-layer meridional circulation.) Finite radiative time constants then allow the temperature perturbations to relax away, leading to a barotropic structure despite the nonzero N^2. Because of the forcing in the top layer, this barotropic structure corresponds to zonal jets with speed u_F.

The link between the present model (with finite $\tau_F^{\rm bot}$) and the barotropic model of Section 2 becomes evident when N^2 is set to zero in Eq. (18). Equation (15) then has the steady-state

solution

$$u = \frac{u_F \Delta p_{\rm top} \tau_F^{\rm bot}}{\tau_F^{\rm bot} \Delta p_{\rm top} + \tau_F^{\rm top} \Delta p_{\rm bot}}, \tag{21}$$

where $\Delta p_{\rm top} = p_{\rm crit} - p_{\rm top}$, $\Delta p_{\rm bot} = p_{\rm bot} - p_{\rm crit}$, $p_{\rm top}$ and $p_{\rm bot}$ are the pressures at the top and bottom of the model, and u_F is the (constant) forcing speed in the upper layer. The model in Section 2 corresponds to letting $\tau_F^{\rm bot} \to \infty$ (i.e., no frictional damping in the bottom layer), in which case $u = u_F$. This explains why u converged to u_F in Fig. 1. In contrast, finite friction timescales in the bottom layer lead to $u < u_F$. As long as $\tau_F^{\rm bot}/\tau_F^{\rm top} \geqslant \Delta p_{\rm bot}/\Delta p_{\rm top}$, however, the equilibrated jet speed u will be a large fraction of u_F.

The time scale for the full system (with nonzero N^2) to reach equilibrium can be investigated by examining the decay rate of an unforced solution with arbitrary initial condition. Because of the linearity of the model, the sum of such a solution and the forced equilibrium solution is the general solution to the forced case with arbitrary initial condition. The free solutions to Eq. (20), with the right-hand side equal to zero, are a series of eigenfunctions with eigenvalues γ_n. The exponential decay rate of mode n is γ_n (always a negative real number). We have examined several cases by numerically searching for roots of the dispersion relation. Eigenfunctions of the streamfunction are displayed in Fig. 6. The two families of modes span the upper and lower layers with increasing numbers of nodes. The fastest relaxation occurs for modes focused near the top (modes 0, 1, 2, 3, 4 in Fig. 6) whereas the slowest relaxation occurs for modes focused near the bottom (modes 30, 31, 32, 33, 34 in Fig. 6). Within each of these branches, the fastest relaxation occurs for the most global modes. In this case the fastest mode relaxes with a time constant of about 2 years, or twice the frictional damping time in the top layer. The factor of two apparently represents the effect of dynamical inertia due to penetration into the deep layer. Models with smaller N show similar character but longer time scales, as the coupling with deeper levels becomes more important.

4. Stably stratified model with thermal forcing

The previous two models considered jets driven solely by an imposed momentum forcing intended to crudely represent momentum-flux convergences caused by the tendency of small-scale eddies to tilt into the jet shear (e.g., Vasavada and Showman, 2005). However, the eddies themselves ultimately result from *thermal* forcing (e.g., convection or baroclinic instabilities). More generally, thermal forcing can play a role when belt-zone contrasts in latent heating or solar-energy absorption produce temperature differences that drive a meridional circulation between belts and zones. Coriolis accelerations on these meridional motions can then drive jets. Here, we consider a simple steady-state, two-layer model of this process analogous to the model in the previous section. Here, the upper layer represents the thermally forced, statically stable upper troposphere, and the lower layer represents the deep interior where heating contrasts are assumed to be minimal. The governing equations are simply Eqs. (15)–(18) with two modifications from our previous treatment: we set u_F to zero in both layers, so that momentum forcing is turned off, and we impose a sinusoidal variation in the latitude dependence of the radiative-equilibrium temperature, T'_E, in the top layer:

$$T'_E = T_0 \sin ly, \tag{22}$$

which imposes belt-zone temperature contrasts on the upper-layer flow. We set T_0 to zero in the bottom layer. Note that the radiative damping and drag terms are retained in both layers. τ_F, τ_R, and NH are again considered piecewise constant in the two layers. When the time-derivative terms are set to zero, Eqs. (15)–(18) admit solutions in u, v, and ψ proportional to $\cos ly$ and in ω and T' proportional to $\sin ly$. Writing $\psi(y, p) = \Psi(p) \cos ly$, the system then collapses to an ordinary differential equation for $\Psi(p)$:

$$\frac{{\rm d}^2\Psi}{{\rm d}p^2} = -\frac{Rl}{f^2\tau_F}\frac{T_0}{p} + \frac{N^2H^2l^2\tau_R}{f^2\tau_F}\frac{\Psi}{p^2}. \tag{23}$$

In the bottom layer ($T_0 = 0$), this equation has polynomial solutions

$$\Psi = A_1 p^{n_1} + A_2 p^{n_2}, \tag{24}$$

where n_1 and n_2 are the two roots of the equation

$$n(n-1) = \frac{N^2H^2l^2\tau_R}{f^2\tau_F}, \tag{25}$$

with the right side specified using parameter values for the bottom layer. The solution in the top layer (which can be obtained by the method of variation of parameters; see Boyce and DiPrima, 1986, pp. 156–158) is

$$\Psi = A_3 p^{n_3} + A_4 p^{n_4} + \frac{RT_0}{N^2H^2\tau_R l}p, \tag{26}$$

where n_3 and n_4 are the roots to Eq. (25) with the right side specified using values for the top layer. Coefficients A_1, A_2, A_3, and A_4 are determined from interface and boundary conditions ($\Psi = 0$ at the top and bottom, and continuity of streamfunction and zonal wind at the interface).

Fig. 7 shows solutions where the stratification is held at a large value ($N = 2 \times 10^{-3}$ s^{-1}) in the top layer and a smaller value in the bottom layer. As with Fig. 4, this provides a crude representation of a stable troposphere overlying a more neutrally stratified interior. To elucidate the behavior, we vary the bottom-layer N over a wide range: N equals 10^{-3} s^{-1} in the top row of panels and is reduced successively by a factor of 10 in the second, third, and fourth (bottom) rows. (The bottom two rows are most relevant to Jupiter.) Scale heights of 25 and 100 km are used in the top and bottom layers. Frictional and radiative time constants are 1 year in the top layer and 1000 years in the bottom layer. The amplitude of thermal forcing, T_0, is set to 5 K (implying 10 K temperature differences between belts and zones). As in Section 3, we adopt $f = 1.8 \times 10^{-4}$ s^{-1} and $l = 5 \times 10^{-7}$ m^{-1}; the top layer extends from 1–5 bars and the bottom layer extends from 5–1000 bars.

Key points are as follows. First, consistent with Fig. 4, the deep region becomes increasingly barotropic as the deep stratification is reduced. Second, all cases show a *reversal* of zonal

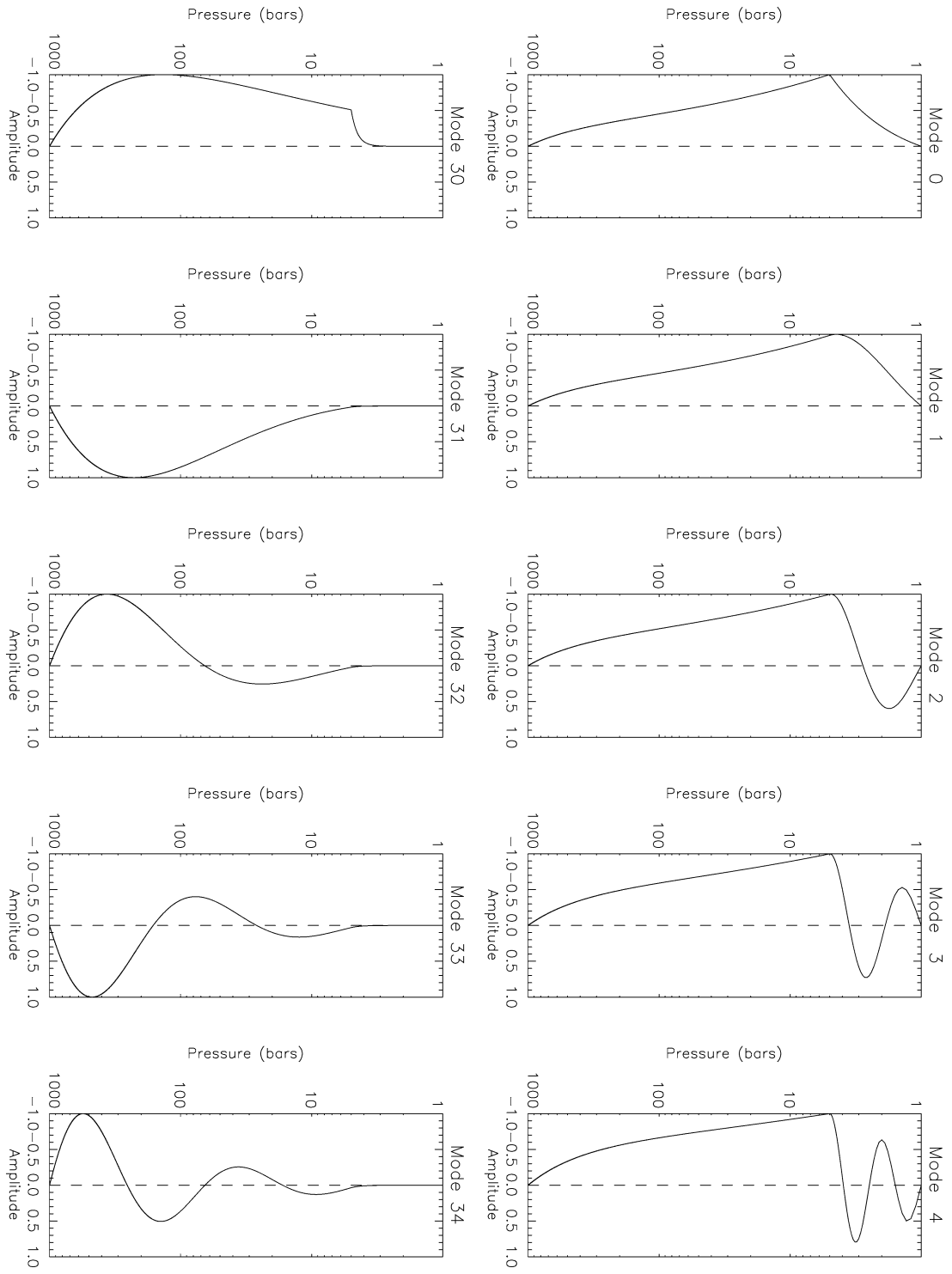

Fig. 6. The structures of a few eigenfunctions are illustrated for the case corresponding to the top row of panels in Fig. 3. See text for discussion.

wind from the top to the bottom (westward at the top and eastward at the bottom or vice versa). This result, which differs from the cases with momentum forcing, *must* occur because the Coriolis acceleration is the only source of jet pumping. Because the meridional circulations form closed cells, the value of v at the top has opposite sign as at the bottom at any given latitude; hence, the Coriolis acceleration drives the jets in the opposite directions at the top and bottom. Third, in the top layer, anticyclonic regions (zones) contain hot, ascending air and cyclonic regions (belts) contain cold, descending air, consistent with the scenario of Ingersoll and Cuzzi (1969). This situation occurs because the thermal forcing is sufficient to overcome the adiabatic cooling (warming) that occurs in ascending (descending) regions. Fourth, as with the model in Section 3, the ratio of frictional time constants in the top and bottom layers plays a key role in allowing deep jets. If the friction time constants are equal

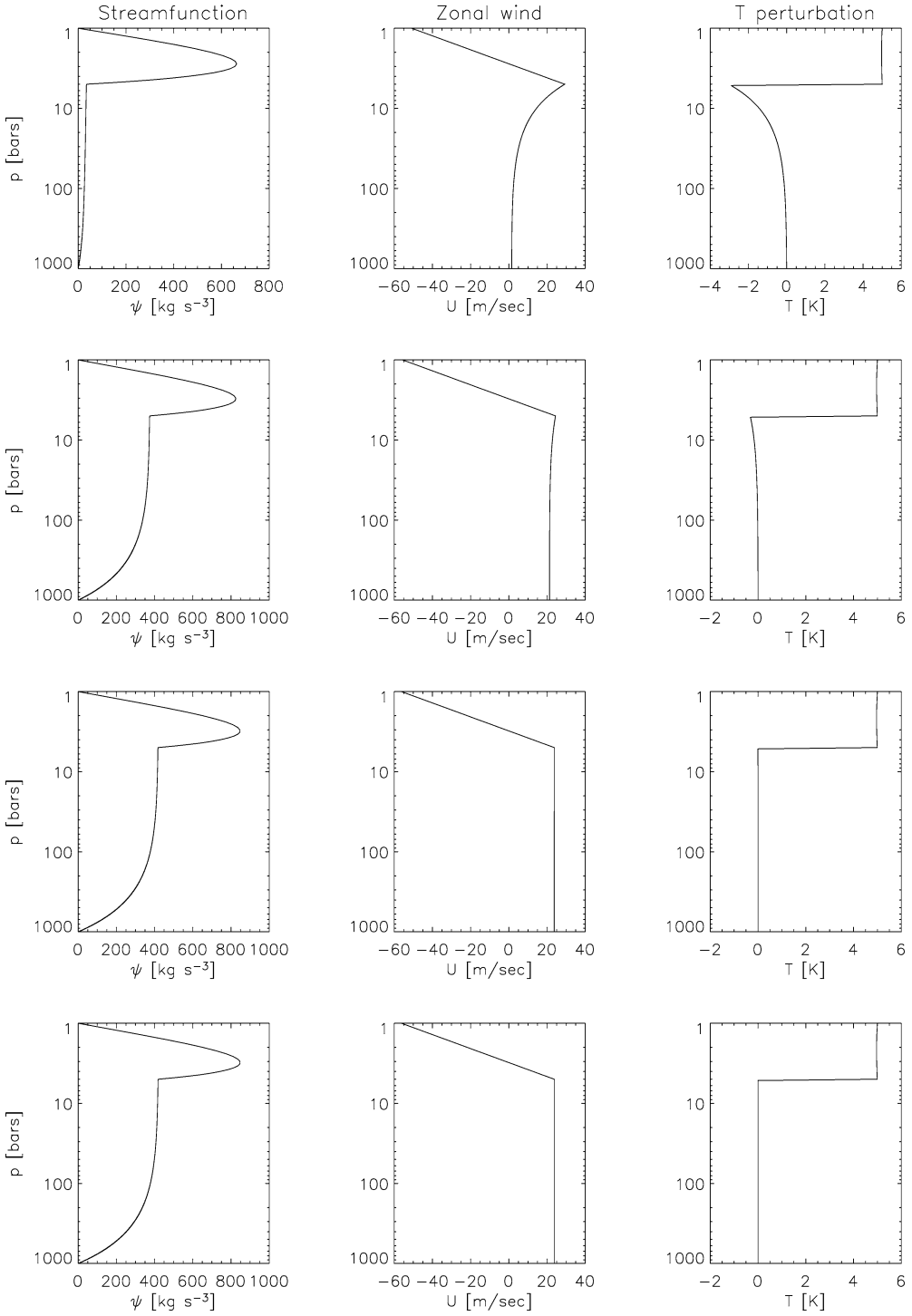

Fig. 7. Effect of static stability on a model with thermal forcing. As in Figs. 3 and 4, each row shows the results of an experiment. In all cases, the Brunt frequency in the top layer is held at $N = 2 \times 10^{-3}$. In the deep layer it is $N = 10^{-3}$, $N = 10^{-4}$, $N = 10^{-5}$, and $N = 10^{-6}$ s^{-1} from top to bottom of the figure. Shown from left to right are the streamfunction Ψ, zonal wind, and temperature perturbation. Even in the presence of a statically stable upper layer, shallow thermal forcing can drive deep jets as long as the deep-layer static stability is small.

in the forced and unforced layers, the deep winds are nearly zero, because the deep-layer values of v (hence jet-pumping east–west Coriolis acceleration) are much less in the deep layer than in the top (forced) layer. Deep jets only exist if the deep friction time constant is at least ∼100 times that in the top layer. As we argued in Section 3, this condition is probably satisfied for Jupiter.

An interesting feature of our most realistic cases (bottom two rows of Figs. 4 and 7) is that, although a deep barotropic wind exists at $p > 5$ bars, it is weaker than the wind at the 1-bar cloud level (by factors of ∼1.3 and 2.4 for the parameter values in Figs. 4 and 7, respectively). At face value, this result seems inconsistent with Galileo probe observations, which exhibited winds that increased from 1–5 bars and remained nearly

constant from 5–20 bars (Atkinson et al., 1997). However, the probe entered the southern edge of an anomalous 5-μm hot spot, and dynamical models strongly suggest that the particular shape of the profile from 1–5 bars results from local dynamics associated with hot spots rather than being a global characteristic of Jupiter's winds (Showman and Dowling, 2000). Numerical simulations of hot spots explain the increasing winds measured by the probe at the southern edge of a hot spot, and they also show that the zonal winds might be constant with depth or even decrease with depth in the middle or northern edge of hot spots (Showman and Dowling, 2000). Therefore, the Galileo probe results do not necessarily contradict the models presented here. It is also possible, however, that a model that includes *both* momentum and thermal forcing could allow profiles like that measured by the Galileo probe to be reproduced; future work can address this issue. Most importantly, we emphasize that the current model is a stripped-down process model intended to demonstrate the basic mechanism by which shallow forcing can induce deep jets in the simplest possible context; it is not intended to match specific wind profiles like that measured by the Galileo probe, which may depend on a variety of factors not included in the model. More advanced models that explore a wider range of vertical stability profiles and include nonlinearity, longitudinal variations, and other factors will allow a better assessment of whether Galileo probe-like wind profiles can be reproduced.

5. Discussion

The models presented here identify a specific mechanism that can induce deep flow from shallow forcing in a giant planet's interior. When jets are forced at the top, an overturning circulation in the meridional (latitude-height) plane develops throughout the depth of the fluid, and Coriolis accelerations on this meridional flow accelerate the jets at *all* depths—not just those that are directly forced. This meridional circulation is ageostrophic, and it results from departures in geostrophy between the zonal wind and geopotential. Nevertheless, its effect is to drive the fluid toward geostrophic balance. When the static stability is large, this geostrophic structure corresponds to jets that extend only slightly into the interior, but small static stabilities lead to barotropic structure where the jets can extend downward to essentially arbitrary depths. Our model excludes diffusion, momentum advection, and dynamical (e.g., inertial or Kelvin–Helmholtz) instabilities, and we emphasize that none of these effects are needed for the development of deep flow from shallow forcing (although in a fully nonlinear model, each of these may contribute to the vertical momentum and energy balance). Instead, the downward energy transport that accelerates the deep jets results from work performed by the upper (forced) layer on the lower (unforced) layer; this work results from the fact that at the interface between these layers, descent occurs where pressure is high and ascent occurs where pressure is low (which causes a downward flux of mechanical energy).

On Jupiter, the shallow-forcing mechanisms that have been proposed involve momentum convergences associated with cloud-level eddies. These eddies may result from moist convection (Ingersoll et al., 2000) or baroclinic instabilities induced by belt-zone temperature contrasts (Williams 1978, 1979, 2002, 2003) that are, in turn, caused by belt-zone variations in latent heating or solar-energy absorption (see Vasavada and Showman, 2005, for a review). Any of these mechanisms would imply the existence of static stability in the layer of jet forcing; Jupiter's adiabatic interior would underlie the forcing level. One of our key results is that even in this situation, deep jets that penetrate the adiabatic molecular region can result. The Galileo probe observation that fast winds extend to pressures >20 bars is therefore equally consistent with either shallow or deep forcing of the jets.

It is interesting to compare our models' predictions of vertical motion with each other and with inferences about Jupiter. In the models with momentum forcing (Sections 2 and 3), ascent occurs in the cyclonic regions (belts) and descent occurs in the anticyclonic regions (zones). In the thermally forced model (Section 4), the signs are reversed. On Jupiter, the cloudiness in zones relative to belts has long suggested that air rises in zones and sinks in belts (e.g., Ingersoll and Cuzzi, 1969). Recently, however, Ingersoll et al. (2000) suggested that, below the clouds, descent occurs in zones and net ascent (primarily in the form of thunderstorms) occurs in belts. Showman and de Pater (2005) showed that this new scenario explains Jupiter's below-cloud ammonia abundances better than the older scenario. The interesting aspect of the rising-in-belts, sinking-in-zones picture of Ingersoll et al. (2000) and Showman and de Pater (2005) is that, within the cloud layer, it requires *equatorward* flow across eastward jets and *poleward* flow across westward jets. The east–west Coriolis accelerations caused by these meridional motions decelerate the jets, so maintenance of the jets in steady state would require eddy-momentum flux convergences (i.e., momentum forcing) that counteract the Coriolis accelerations. Thus, inferences on vertical motion hint that, at cloud level, the jets are indeed driven by eddy-flux convergences rather than Coriolis accelerations on the meridional flow of zonally symmetric Hadley cells.

Because of the sinusoidal nature of the solutions presented here, the eastward and westward jets in our models have equal strengths, implying that the net angular momentum is zero relative to the rotating reference frame. Jupiter's observed cloud-level jets, however, have net eastward momentum relative to the magnetic-field rotation rate (System III, which presumably represents the rotation rate of the deep interior). The mechanisms that produce the net eastward cloud-level flow remain obscure, although they presumably involve fluid-dynamical torques, resulting from turbulence or waves, between the cloud-layer and deeper flows. This process could potentially be parameterized in our model by adding sources of eastward and westward momentum in the top and bottom layers, respectively, but we do not expect that such an addition would qualitatively alter our results. A satisfying explanation of this puzzle, as well as the more fundamental puzzle of whether the jets are primarily driven in the cloud layer or deep interior, will require a new generation of nonlinear, three-dimensional numerical simulations of Jupiter's interior flow that are constrained by available observations.

Acknowledgments

This work was supported by the NASA Planetary Atmospheres program through Grant no. NAG5-13329 and the NSF Planetary Astronomy program through Grant AST-0306955. We thank the Cornell Astronomy Department for hosting A.P.S. during the course of this project.

References

Achterberg, R.K., Ingersoll, A.P., 1989. A normal-mode approach to jovian atmospheric dynamics. J. Atmos. Sci. 46, 2448–2462.

Allison, M., 1990. Planetary waves in Jupiter's equatorial atmosphere. Icarus 83, 282–307.

Allison, M., 2000. A similarity model for the windy jovian thermocline. Planet. Space Sci. 48, 753–774.

Allison, M., Atkinson, D.H., 2001. Galileo probe Doppler residuals as the wave-dynamical signature of weakly stable, downward-increasing stratification in Jupiter's deep wind layer. Geophys. Res. Lett. 28, 2747–2750.

Atkinson, D.H., Pollack, J.B., Seiff, A., 1996. Galileo Doppler measurements of the deep zonal winds at Jupiter. Science 272, 842–843.

Atkinson, D.H., Ingersoll, A.P., Seiff, A., 1997. Deep zonal winds on Jupiter: Update of Doppler tracking the Galileo probe from the orbiter. Nature 388, 649–650.

Atkinson, D.H., Pollack, J.B., Seiff, A., 1998. The Galileo probe Doppler wind experiment: Measurement of the deep zonal winds on Jupiter. J. Geophys. Res. 103, 22911–22928.

Aurnou, J.M., Olson, P.L., 2001. Strong zonal winds from thermal convection in a rotating spherical shell. Geophys. Res. Lett. 28, 2557–2560.

Barcilon, A., Gierasch, P., 1970. A moist, Hadley cell model of Jupiter's cloud bands. J. Atmos. Sci. 27, 550–560.

Bartello, P., Holloway, G., 1991. Passive scalar transport in β-plane turbulence. J. Fluid Mech. 223, 521–536.

Beebe, R.F., Ingersoll, A.P., Hunt, G.E., Mitchell, J.L., Miller, J.P., 1980. Measurement of wind vectors, eddy momentum transports, and energy conversions in Jupiter's atmosphere from Voyager 1 images. Geophys. Res. Lett. 7, 1–4.

Bosak, T., Ingersoll, A.P., 2002. Shear instabilities as a probe of Jupiter's atmosphere. Icarus 158, 401–409.

Boyce, W.E., DiPrima, R.C., 1986. Elementary Differential Equations and Boundary Value Problems, fourth ed. Wiley, New York.

Busse, F.H., 1976. A simple model of convection in the jovian atmosphere. Icarus 29, 255–260.

Christensen, U.R., 2001. Zonal flow driven by deep convection in the major planets. Geophys. Res. Lett. 28, 2553–2556.

Christensen, U.R., 2002. Zonal flow driven by strongly supercritical convection in rotating spherical shells. J. Fluid Mech. 470, 115–133.

Cox, J.P., Giuli, R.T., 1968. Principles of Stellar Structure, vol.1: Physical Principles. Gordon & Breach, New York.

Fernando, H.J.S., Chen, R.-R., Boyer, D.L., 1991. Effects of rotation on convective turbulence. J. Fluid Mech. 228, 513–547.

Flasar, F.M., Gierasch, P.J., 1986. Mesoscale waves as a probe of Jupiter's deep atmosphere. J. Atmos. Sci. 43, 2683–2707.

Folkner, W.M., Preston, R.A., Border, J.S., Navarro, J., Wilson, W.E., Oestreich, M., 1997. Earth-based radio tracking of the Galileo probe for Jupiter wind estimation. Science 275, 644–646.

Friedson, A.J., 2005. Water, ammonia, and H_2S mixing ratios in Jupiter's five-micron hot spots: A dynamical model. Icarus 177, 1–17.

Gierasch, P.J., 1973. Jupiter's cloud bands. Icarus 19, 482–494.

Gierasch, P.J., 1976. Jovian meteorology: Large-scale moist convection. Icarus 29, 445–454.

Gierasch, P.J., Ingersoll, A.P., Williams, R.T., 1973. Radiative instability of a cloudy planetary atmosphere. Icarus 19, 473–481.

Holton, J.R., 2004. An Introduction to Dynamic Meteorology, fourth ed. Elsevier, Amsterdam. 535 pp.

Ingersoll, A.P., Cuzzi, J.N., 1969. Dynamics of Jupiter's cloud bands. J. Atmos. Sci. 26, 981–985.

Ingersoll, A.P., Kanamori, H., 1995. Waves from the collisions of Comet Shoemaker–Levy 9 with Jupiter. Nature 374, 706–708.

Ingersoll, A.P., Beebe, R.F., Mitchell, J.L., Garneau, G.W., Yagi, G.M., Müller, J.-P., 1981. Interaction of eddies and mean zonal flow on Jupiter as inferred from Voyager 1 and 2 images. J. Geophys. Res. 86, 8733–8743.

Ingersoll, A.P., Gierasch, P.J., Banfield, D., Vasavada, A.R., the Galileo imaging team, 2000. Moist convection as an energy source for the large-scale motions in Jupiter's atmosphere. Nature 403, 630–632.

Ingersoll, A.P., Dowling, T.E., Gierasch, P.J., Orton, G.S., Read, P.L., Sanchez-Lavega, A., Showman, A.P., Simon-Miller, A.A., Vasavada, A.R., 2004. Dynamics of Jupiter's atmosphere. In: Bagenal, F., Dowling, T.E., McKinnon, W.B., Jewitt, D., Murray, C., Bell, J., Lorenz, R., Nimmo, F. (Eds.), Jupiter: Planet, Satellites, and Magnetosphere. Cambridge Univ. Press, New York, pp. 105–128.

Johnson, T.V., 2000. The Galileo mission to Jupiter and its moons. Sci. Am. 282 (2), 40–49.

Kalnay, E., 2003. Atmospheric Modeling, Data Assimilation, and Predictability. Cambridge Univ. Press, New York.

Magalhães, J.A., Seiff, A., Young, R.E., 2002. The stratification of Jupiter's troposphere at the Galileo probe entry site. Icarus 158, 410–433.

Nakajima, K., Takehiro, S.-I., Ishiwatari, M., Hayashi, Y.-Y., 2000. Numerical modeling of Jupiter's moist convection layer. Geophys. Res. Lett. 27, 3129–3132.

Ortiz, J.L., Orton, G.S., Friedson, A.J., Stewart, S.T., Fisher, B.M., Spencer, J.R., 1998. Evolution and persistence of 5-micron hot spots at the Galileo probe entry latitude. J. Geophys. Res. 103, 23051–23069.

Pollack, J.B., Atkinson, D.H., Seiff, A., Anderson, J.D., 1992. Retrieval of a wind profile from the Galileo probe telemetry signal. Space Sci. Rev. 60, 143–178.

Salyk, C., Ingersoll, A.P., Lorre, J., Vasavada, A.R., Ewald, S., Del Genio, A.D., 2006. Interaction between eddies and mean flow in Jupiter's atmosphere: Analysis of Cassini imaging data. Icarus. In press.

Seiff, A., 2000. Dynamics of Jupiter's atmosphere. Nature 403, 603–604.

Seiff, A., Blanchard, R.C., Knight, T.C.D., Schubert, G., Kirk, D.B., Atkinson, D., Mihalov, J.D., Young, R.E., 1997. Wind speeds measured in the deep jovian atmosphere by the Galileo probe accelerometers. Nature 388, 650–652.

Seiff, A., Kirk, D.B., Knight, T.C.D., Young, R.E., Mihalov, J.D., Young, L.A., Milos, F.S., Schubert, G., Blanchard, R.C., Atkinson, D., 1998. Thermal structure of Jupiter's atmosphere near the edge of a 5-μm hot spot in the north equatorial belt. J. Geophys. Res. 103, 22857–22889.

Showman, A.P., Dowling, T.E., 2000. Nonlinear simulations of Jupiter's 5-micron hot spots. Science 289, 1737–1740.

Showman, A.P., de Pater, I., 2005. Dynamical implications of Jupiter's tropospheric ammonia abundance. Icarus 174, 192–204.

Turner, J.S., 1979. Buoyancy Effects in Fluids. Cambridge Univ. Press, New York.

Vasavada, A.R., Showman, A.P., 2005. Jovian atmospheric dynamics: An update after Galileo and Cassini. Rep. Prog. Phys. 68, 1935–1996.

Williams, G.P., 1978. Planetary circulations. 1. Barotropic representations of jovian and terrestrial turbulence. J. Atmos. Sci. 35, 1399–1426.

Williams, G.P., 1979. Planetary circulations. 2. Jovian quasi-geostrophic regime. J. Atmos. Sci. 36, 932–968.

Williams, G.P., 2002. Jovian dynamics. Part II. The genesis and equilibration of vortex sets. J. Atmos. Sci. 59, 1356–1370.

Williams, G.P., 2003. Jovian dynamics. Part III. Multiple, migrating, and equatorial jets. J. Atmos. Sci. 60, 1270–1296.

Young, R.E., 2003. The Galileo probe: How it has changed our understanding of Jupiter. New Astron. Rev. 47, 1–51.